original copy

83N13394

DEPARTMENT OF
ENGINEERING SCIENCES

College of Engineering
University of Florida Gainesville, FL 32611

THE INVESTIGATION OF FLOW INSTABILITIES ON A ROTATING DISK WITH CURVATURE IN THE RADIAL DIRECTION

FINAL REPORT

for the period

October 1, 1980 through December 31, 1981

by

Paul A. Intemann, Graduate Student

and

Mark H. Clarkson, Principal Investigator

Department of Engineering Sciences
University of Florida
Gainesville, Florida 32611

NASA Technical Officer for this Research Grant
is Mr. Steve Wilkinson, Langley Research Center,
Hampton, Virginia 23665

Research Grant No. NAG-1-104

Date: December 14, 1982

"Page[s] missing from available version"

I THRU III

TABLE OF CONTENTS

LIST OF TABLES

LIST OF FIGURES

TABLE OF SYMBOLS

A	Paraboloid constant, 6.944×10^{-2}
N	Number of vortices visible around the circumference of the test body at a specified radius
r	Radial coordinate
r_o	Radial distance at which instability first becomes visible
r_t	Radial distance at which transition from vortex system to turbulent flow occurs
R_c	Crossflow Reynolds number
R_r	Reynolds number = $r^2\omega/\nu$
R_{δ_1}	$1.271\sqrt{R_r}$
R_{r_o}	Reynolds number at which the instabilities first become visible
R_{r_t}	Reynolds number at which transition to turbulent flow occurs
s	Distance along the curved surface of the paraboloids (see Fig. 8)
s_o	Distance along the curved surface of the paraboloids at which instability becomes visible (see Fig. 8)
t	Thickness of test body
u	Local velocity inside the boundary layer
V_c	Maximum crossflow velocity component due to secondary flow in the boundary layer (perpendicular to flow outside the boundary layer)
V_t	Tangential velocity component
y	Coordinate normal to the flat surface of the test body
z	Coordinate in the circumferential direction on the top flat surface of the test body
α	Non-dimensional wave number
δ_1	Boundary layer displacement thickness

ε Angle between the normal to the vortex axis and the radius of the test body (see Fig. 2)

λ_α Vortex spacing measured normal to the vortex axis

$\overline{\lambda}_\alpha$ λ_α/δ_1

λ_ϕ Vortex spacing in circumferential direction at a given radius

η Number of timing marks on film per film frame

ζ Number of film frames per test body revolution

ω Rotational speed of test body

ν Kinematic viscocity

SECTION I
INTRODUCTION

The flow development about a rotating disk immersed in a fluid has been the subject of numerous investigations over the past 60 years.

In 1921 Theodore von Karman[1] obtained the exact solution of the steady state Navier-Stokes equations for an infinite disk rotating in a fluid. Then, in 1934, W. G. Cochran[2] was the first to carry out a numerical integration of the solution obtained by von Karman and to show the nature of the boundary layer profiles in the radial and circumferential directions (see Figure 1).

In 1947, Smith[3] carried out an investigation on a flat rotating disk by the use of a hot-wire probe. Radial traverses of the disk exhibited an onset of periodic fluctuations (approximately 32 oscillations per disk revolution) of the probe output at approximately the same local Reynolds number, $\sqrt{R_r}$, regardless of rotational speed of the disk. As the traverses were continued radially outward the fluctuations suddenly became random, again at a local Reynolds number that did not change with variations of the rotational velocity of the disk. The disturbance wavefronts were calculated by Smith to be oriented at an angle ε of 14° with respect to the outward drawn radius (see Figure 2).

During early flight testing of airplanes with swept-back wings it was visually observed that the point of transition from laminar to turbulent flow on the wing was located much further forward than anticipated.[4] Owen and Randall,[5] in their wind tunnel tests of swept-

back wings, attempted to explain the observed phenomenon. They attributed the vortex formation they discovered in the region of transition from laminar to turbulent flow to instabilities in the laminar boundary layer and hypothesized that these instabilities had been caused by the inflexional nature of the boundary layer profile in the direction normal to the local free-stream velocity vector.

The rotation of a disk at a constant angular velocity in a fluid initially at rest leads to the development of a radial velocity profile which exhibits precisely such a point of inflexion. This similarity to the velocity profile observed over swept-back wings and the availability of the exact solution of the velocity profiles for use in stability analysis along with the experimental simplicity in studying rotating disk flow prompted further extensive experimental and theoretical investigations.

Gregory et al.[6] were the first to make visible the vortex pattern responsible for the periodic fluctuations recorded by Smith.[3] The china-clay technique was employed to visualize the flow field and it showed that the vortex pattern observed was stationary with respect to the disk. The investigators were thus able to offer the following explanation as to how the flow field developed: A laminar flow field is observed up to a certain radius (this radius being a function of the rotational velocity of the disk), further out on the disk the vortical flow pattern appears and radially beyond these vortices the flow becomes turbulent (the location again dependent on the rotational velocity of the disk). A hot-wire probe was also utilized by the investigators to obtain such pertinent flow parameters as ε, λ_ϕ, $\sqrt{R_{r_o}}$, and $\sqrt{R_{r_t}}$. The Reynolds number at which the vortex system appeared was found to be

$\sqrt{R_{r_o}} \simeq 430$ while turbulence usually occured at $\sqrt{R_{r_t}} \simeq 530$. The angle ε was found to be equal to 14° and 32-33 vortices were detected during one revolution of the disk, both values being almost identical to those attained by Smith.[3]

In 1966, tests were carried out by Faller and Kaylor[7] utilizing dyes in water as a means of visualizing the flow field. In this investigation a circular water tank was brought to a constant rotational velocity and spun long enough for the water and tank to essentially turn as a rigid body. Then the rotational velocity of the tank was suddenly increased to a new value causing the flow at the bottom of the tank to behave essentially like rotational disk flow, once acceleration transients had died out. Chin and Litt[8] in 1972 experimentally investigated the behavior of fluid motion in the neighborhood of a rotating disk by implanting electrochemical probes into a flat Lucite disk to determine turbulence transition radii and the presence of surface vortices. These cathodic point electrodes, in conjunction with anodes suspended below the disk, yielded a different current fluctuation depending upon the position of the probe in the flow field - laminar, transition, or turbulent - and on the rotational velocity of the disk. The results obtained by both investigations are summarized in Table 1 and compare favorably with those calculated by Gregory et al.[6] The two most recent investigations carried out were done by Kobayashi et al.[9] and Malik et al.[10] Both groups of experimenters chose hot-wire anemometers to investigate the flow field. The $\sqrt{R_{r_o}}$ reported by both groups was much lower ($\sqrt{R_{r_o}} \simeq 295$) than reported by any previous investigation, while $\sqrt{R_{r_t}}$ was generally in close agreement with earlier results. Both investigations found a slow variation of ε with $\sqrt{R_r}$ and agreed that the number of vortices present circumferentially increased with $\sqrt{R_r}$.

Gregory et al.[6] carried out a theoretical analysis of the observed flow instability concurrent with their experimental work, but neglected viscous effects and thus predicted 113-140 vortices around the circumference of the disk instead of the observed 30-32 vortices. Brown,[11] in a later study, took viscocity into account and found $\sqrt{R_{r_o}} \tilde{=} 178$, much less than that observed experimentally. Next, Tobak[12] calculated the vortex spacing and inclination angle ε taking into account viscocity and in the case of vortex inclination, obtained close agreement with experimental results of Clarkson et al.[13] while the vortex spacing was comparable to that calculated by Gregory et al.[6] The theortetical work carried out by Kobayashi et al.[9] and Malik et al.[10] predicted a critical Reynolds number $\sqrt{R_{r_o}}$ of 287 and 261, respectively, by taking into account in the calculations coriolis forces and streamline curvature. As can be seen from Table 1 this compared favorably with the experimental results found by both investigators.

It is thus clear that considerable effort has gone into the experimental and theoretical investigation of the described flow phenomena during the past six decades. The major objective of the present work is to explore any visible differences of the flow field with wall curvature of the test body, including possible interaction between Taylor-Gortler instabilities present along concave walls and the inflexional instabilities investigated here.

SECTION II
EXPERIMENTAL INVESTIGATION

An experimental study was conducted with emphasis placed on making visible and recording photographically the flow instabilities present under three different rotating bodies: a flat disk, a concave paraboloid, and a convex paraboloid.

Rotating Disk and Paraboloid Apparatus

The bodies under investigation were mounted on a vertical shaft which was driven by a drill motor through a 2:1 gearing belt. A rheostat was utilized to vary the rotational velocity of the shaft.

The water used to visualize the flow pattern under investigation was contained in a 4 x 4 x 1.5 ft. plexiglass box and was kept at a height of 11.5 in. during test runs. Test bodies were semi-immersed in the water in such a way that only the bottom of each came in contact with the water. This made it possible to observe the flow field by looking downward through the body tested.

The camera used in recording the test runs was mounted on a heavy-duty tripod and positioned as shown in Figure 3. To avoid having to suspend the camera from the ceiling directly above the test body, a front surface mirror was mounted in the position shown. Thus, photographing the test runs from ground level was possible.

Due to the high film speeds utilized in photographing the flow field, three 1000 watt - 3200 °K quartz iodine lamps were used to illuminate the test bodies while filming. The position of each lamp relative to the bodies tested was chosen to minimize reflective glare.

Test Bodies

A total of three geometrically distinct bodies were constructed and tested to gain insight into the variation of the flow field with wall curvature.

The flat disk, shown in Figure 4, had a diameter of 24 in., was 0.5 in. thick, and made out of clear plexiglass. Radial lines at 15° intervals and concentric circles spaced 1 in. apart were drawn onto the top of the disk to facilitate data reduction from the motion picture film. Results obtained from this disk were used for comparison with earlier results obtained investigating this same disk in a different water tank.[13]

Experimental work was carried out at the NASA Langley research center on an 18-in. diameter, 5-in. deep metallic concave paraboloid. NASA investigators were particularly interested in the development of the flow field and vortex pattern along a surface with curvature such as exists at wing-body junctures on airplanes. Since these tests were conducted in air rather than water, the decision was made to conduct test runs in the water tank utilizing an equally sized plexiglass test body to compare results. For maximum cost effectiveness, six 1-in. thick clear plexiglass plates were glued together and then machined to the desired concave shape. The largest diameter lathe available for making the concave paraboloid was too small to machine it to the same size as the one tested at NASA Langley. It was thus decided that the equation according to which the paraboloid was to be cut be modified to keep it geometrically similar to the metallic paraboloid. The concave paraboloid and the equation according to which it was machined is shown in Figure 5. To aid in data reduction the flat surface of the test body

was marked by four thin strips of white tape placed 90° apart and marked radially at 1 in. intervals on the tape. In addition, the side of the disk was painted black to cut down on undesirable reflections.

The convex paraboloid was also machined after cementing together six plexiglass plates. In a manner similar to the concave paraboloid, the flat surface of this test body was also marked with tape. From Figure 6 it can be seen that the convex paraboloid was machined in such a way as to be a male-female match for the concave paraboloid.

Test Procedures

The investigation was initiated by first testing the flat disk in an aluminum particle-water mixture. By using a suitable wetting agent it was possible to suspend 30 μ diameter aluminum particles uniformly in water at a ratio of 200:1 by weight. The resulting mixture gave excellent indications of the areas of laminar, turbulent, and transitional flow. The vortex pattern was visible the moment the disk was set in motion. A Nova model 16-3 motion picture cammera, capable of framing rates between 400 and 10,000 frames per second, in conjunction with a Zoomar Zoomatar f2.8/90 lens with tube extension was used to film these initial test runs. A previous investigation[13] of this same disk had been made using maximum framing rates of 300 frames per second. The Nova camera used was thus able to increase four to five-fold the framing rate while at the same time yielding results that could be compared to data collected by Clarkson et al.[13] The film used in photographing the test runs was Kodak 400 ASA 16 mm B/W positive reversal film. While it delivered results suitable for data reduction, the lack of resolution of the individual film frames prompted the decision to switch to Kodak 400 ASA 16 mm B/W negative film. This was also done in anticipation of

having enlargements made from single frames of interest, thereby possibly increasing the resolution over that achieved with the positive reversal film.

The next body to be tested was the concave paraboloid. Unfortunately, it was impossible to achieve any acceptable results using either of the aforementioned films. Every test run carried out yielded a completely underexposed film, regardless of the positioning of the three floodlights. Since, up to this point in the investigation, framing rates of 1400 to 1500 frames per second had been used, it was decided that the framing rate be lowered to allow for correct exposure of the concave paraboloid test runs. When this attempt again yielded underexposed film, a switch to a different camera and film was made. Likewise, a different means of visualizing the flow field was resorted to. The aluminum particle-water mixture was discarded and replaced by tap water. A dye-injection nozzle was constructed which allowed sodium fluorescein dye to be injected anywhere underneath the test body (see Figure 3). A Locam model 51 16-mm intermittent pin-registering camera with a Polaris f2 18-90 mm zoom lens and short tube extension was used together with Kodakcolor 400 ASA 16 mm television news film to record the rest of the investigation. The switch to color film was made due to the enhanced contrast it offered between the clear water and the green dye as compared to the black-and-white film.

Test runs utilizing the dye-injection apparatus were carried out as follows: After the tank was filled with tap water and the turbulence had settled, the sodium fluorescein dye was injected directly under the concave paraboloid. By placing the injector nozzle at the correct location the dye would follow a spiraling path along the underside of

the body and be convected outward by the radial velocity component into the field of view (FOV) of the camera. If, concurrently, the rotational velocity of the concave paraboloid was such that the vortex system was present underneath the body in the FOV of the camera, these vortices would trap and concentrate the dye to show the expected instability in the flow field. Following each test run, the water tank was flushed out and refilled with fresh tap water. This same visualization technique was employed in testing the convex paraboloid.

Data Reduction

All relevant data necessary to calculate the results given in Table 1 were collected from the 16 mm film used to record the test runs. Since both cameras employed in the investigation included internal devices which generated indicator marks on the edge of the film strips, framing rates were simply and accurately calculated by counting frames between adjacent marks and multiplying this number by 120 for films exposed with the Nova camera and 100 for the Locam camera.

The rotational velocity of the test bodies was calculated by counting the number of frames elapsed for one revolution of the body and dividing this number by the calculated film speed. The inverse of the result yielded the rotational speed in revolutions per second.

The photographic results obtained during the test runs were used primarily to acquire reliable data on ε and α. A Kodak photo-data-analyzer projector was utilized to freeze frames in which the vortex pattern was clearly visible and ε was then measured directly off the screen by setting up tangents to the vortex and the circumferentially marked lines on the test bodies and measuring the angle between the two lines. Likewise, α was found by measuring the circumferential distance

between adjacent vortex lines. At least three readings of α and ε were taken at various locations on the film for each test run. The accuracy of the readings for ε were approximately $\pm$ 0.5°.

Angle Correction on Paraboloids

When measured on either the concave or convex paraboloid, ε was actually foreshortened due to the curvature of the bodies. Calculations for correcting ε are given below and a comparison between measured and corrected ε can be found in Table 8.

ε_m - Angle of inclination of vortex as measured off the photographic data. (see Figure 7)

ε_c - Actual angle of inclination of vortex with respect to the disk. (see Figure 7)

The equation of the convex disk is given by

$$y = Ar^2 \ . \tag{1}$$

Differentiating,

$$\frac{dy}{dr} = 2Ar = \tan \alpha \ , \text{ and} \tag{2}$$

thus

$$\alpha = \tan^{-1} \left. \frac{dy}{dr} \right|_{r = r_o} \ . \tag{3}$$

From Figure 7,

$$\tan \varepsilon_c = \frac{ds}{dz} \ , \text{ a} \tag{4}$$

$$\tan \varepsilon_m = \frac{dr}{dz} \ , \text{ and} \tag{5}$$

$$\sin \alpha = \frac{dy}{ds} \ . \tag{6}$$

Combining 3, 4, 5, and 6 yields

$$\varepsilon_c = \tan^{-1} \frac{\tan \varepsilon_m}{\cos \alpha} \text{ , where } \alpha = \tan 2Ar_o \text{ .} \quad (7)$$

Radial Distance Correction for Paraboloids

For the convex and concave paraboloids the local Reynolds number $\sqrt{R_{r_o}}$ was corrected by calculating it using the arc length s rather than r as shown in Figure 8. The calculation of s_o knowing r_o was done as follows:

From Figure 8,

$$(dr)^2 + (dy)^2 = (ds)^2 \text{ ,} \quad (8)$$

$$ds = \left[(dr)^2 + (dy)^2\right]^{1/2} = \left[(dy/dr)^2 + 1\right]^{1/2} dr \text{ , and} \quad (9)$$

$$\int_o^{s_o} ds = \int_o^{r_o} \left[(dy/dr)^2 + 1\right]^{1/2} dr \text{ .} \quad (10)$$

Since

$$y = Ar^2 \text{ and } \frac{dy}{dr} = 2Ar \text{ , then}$$

$$s_o = \int_o^{r_o} \left[4A^2r^2 + 1\right]^{1/2} dr \text{ , and} \quad (11)$$

$$s_o = \frac{r_o\left(4A^2r_o^{\,2} + 1\right)^{1/2}}{2} + \frac{1}{4A} \ln \left(2Ar_o + \left(4A^2r_o^{\,2} + 1\right)^{1/2}\right). \quad (12)$$

Table 9 gives a comparison between a given r_o and its corresponding s_o.

Experimental Results

A crossflow Reynolds number R_c was first defined by Owen and Randall[5] in an attempt to correlate their data. They reasoned that R_c should be a function of the secondary flow component and the boundary layer displacement thickness and defined a crossflow Reynolds number to be

$$R_c = \frac{V_c \delta_1}{\nu} . \tag{13}$$

For the rotating bodies tested, the secondary flow component is the radial velocity. Von Karman,[1] in his solution of fluid flow near a flat disk, showed that

$$V_c = 0.181\ r\omega \quad \text{and} \tag{14}$$

$$\delta_1 = 1.271\sqrt{\nu/\omega} . \tag{15}$$

Substitution of 14 and 15 into 13 yields

$$R_c = 0.230 \frac{r\omega}{\nu} \frac{\nu}{\omega}^{1/2} = 0.230 \left[\frac{r^2\omega}{\nu}\right]^{1/2} = 0.230\sqrt{R_r} . \tag{16}$$

An alternate Reynolds number proposed by Owen and Randall[5] was based, not on the crossflow velocity, but on the tangential velocity component

$$V_t = r\omega . \tag{17}$$

Substitution of 15 and 17 into 13 yields

$$R_{\delta_1} = \frac{r\omega\delta_1}{\nu} = 1.271 \left[\frac{r^2\omega}{\nu}\right]^{1/2} = 1.271\sqrt{R_r} . \tag{18}$$

The spacing between vortices measured along the circumference of the disk at a specified radius r is given by

$$\lambda_\phi = \frac{2\pi r}{N} \tag{19}$$

where N is the number of vortices. Spacing normal to the vortex is given by

$$\lambda_\alpha = \lambda_\phi \sin \varepsilon = \frac{2\pi r}{N} \sin \varepsilon \, . \tag{20}$$

Nondimensionalizing λ_α by dividing by δ_1 yields

$$\bar{\lambda}_\alpha = \frac{\lambda_\alpha}{\delta_1} = \frac{\lambda_\alpha}{1.271(\nu/\omega)^{1/2}} = \left[\frac{w}{\nu}\right]^{1/2} \frac{2\pi r \sin \varepsilon}{1.271N} \tag{21}$$

$$= \frac{2\pi \sin \varepsilon}{1.271N} \sqrt{R_r} \, . \tag{22}$$

Finally, a non-dimensional wave number may be defined by

$$\alpha = \frac{\bar{\lambda}_\alpha}{2\pi} \tag{23}$$

for a two-dimensional disturbance propagating along a line normal to the vortex axis. Data of previous experimental work as well as quantities obtained in this experimental investigation are presented in Tables 1, 5, 6 and 7.

SECTION III
RESULTS AND DISCUSSION

The vortex pattern visible in Figures 9 and 10 are typical of the vortices present under the flat disk. Both prints, taken with a 35 mm Canon F-1 camera, were not used for data reduction but presented since they clearly show the sodium fluorescein dye evenly distributed in the region under the disk where the flow is laminar. At r = 7.6 in. the vortex pattern becomes visible and fully turbulent flow is attained at r = 9.4 in. Figure 10 also illustrates how fluctuating the pattern can be. On the left side of the print, the flow is fully turbulent at r = 8.5 inches while on the right the vortex pattern remains intact up to a radius of r = 9.4 inches. Figures 9 and 10 show the vortex pattern made visible by use of the dye in water technique, whereas, Figures 11 and 12 are enlargements made from 16 mm Kodak 400 ASA negative reversal film of the flat disk used in conjunction with the aluminum particle-water mixture. Note the two vortex filaments visible in the middle of Figure 11 and how they appear to move further apart as they move radially inward.

From the data presented in Table 1 a noticeable variation in Reynolds numbers for instability and transition is apparent. The reason for this probably lies with the different test procedures utilized in each investigation or external disturbances that influenced the test results. It is interesting to note, though, that the values of $\sqrt{R_{r_o}}$ and $\sqrt{R_{r_t}}$ found by Gregory et al.[6] and Chin and Litt[8] are almost identical to

those found in this investigation even though three different test methods were employed. Also, the difference between the results for the flat disk in this investigation and those gotten by Clarkson et al.[13] in an earlier test of the same disk should be noted. The reason for the variation in Reynolds numbers between these two tests is most probably due to the different-sized water tanks used in the investigations. The test runs carried out by Clarkson et al.[13] were done in a 10 ft. deep vertical water tunnel with the model submerged to a depth of 1 ft. while the present results were obtained in a 1 ft. deep water tank. The possibility of re-circulating water influencing the results obtained in this shallow water tank does exist since a circulating flow was usually present in the tank when the disk was stopped after long test runs. Therefore, a further investigation into the variation of test results with water depth would be indicated. Likewise, the fact that the current test runs on the flat disk were carried out using the aluminum particle-water mixture as a means of visualizing the flow field rather than the sodium fluorescein dye injection method used by Clarkson et al.[13] may have influenced the results. In previous investigations of flow instabilities on rotating disks, the value of ε, the angle between the normal to the vortex axis and the radius of the disk, has always been a point of uncertainty. While, for instance, Clarkson et al.[13] reported measuring a value of 11°, Gregory et al.[6] gave a figure of 14°. As can be seen from Table 2 it is apparent that for the flat disk ε varies with r for constant Reynolds number. Similar observations were made by Kobayashi et al.[9] using a hot-wire probe investigative method and lead to the conclusion that the behavior observed in ε during the testing of the flat disk was not influenced by the type of flow

visualization technique employed. A similar behavior in ε was not detected on the paraboloid test bodies since sodium fluorescein dye rather than the aluminum particle-water mixture had to be used, as discussed earlier, to make visible the vortex pattern. Since, when using the aluminum particle-water mixture, the pattern instantaneously appeared at any radial position on the flat disk depending only on ω, it was relatively easy to detect a variation of ε with r_o. Making the instability appear at various radii on the paraboloids proved to be extremely difficult due to the complicated test procedure necessary to cause the vortex pattern to appear in the field of view of the camera. Thus, further investigation of the paraboloid test bodies, using the aluminum particle-water mixture to visualize the flow field for variation of ε with r_o should be seriously considered by future investigators.

Both Faller and Kaylor[7] and Malik et al.[10] reported finding an instability mechanism different from the stationary disturbances investigated here. This flow phenomena, which was called Type II instabilities by Faller and Kaylor,[7] first appeared at much lower Reynolds numbers, $R_c \tilde{=} 50$ and had negative values for ε. While this type of instability was not detected during this investigation with any regularity, it was photographed on a number of occasions. When it was observed, it could be seen propagating outward and interfering destructively with the stationary vortex pattern under investigation. An example of both patterns visible simultaneously under the flat disk can be seen in Figure 13. The two distinct patterns visible in this picture were observed during Test Run 3. The pattern at the bottom of the figure was caused by the Type II instabilities first observed in

reference 7, while the one seen at the top of the photograph is the instability also seen in Figures 9, 10, 11 and 12. While an $\sqrt{R_{r_o}}$ was not calculated for this type of instabillity because the r_o at which the disturbance first appeared was always outside the field of view of the camera, ε did decrease with Reynolds number as reported by Faller and Kaylor.

A similar type of instability was observed during the testing of the convex paraboloid. Figures 14, 15 and 16 are enlargements made from the 16 mm color film and show a progression of events as they occurred during Test Run 3. Figure 14 shows the streaks of dye for laminar flow, while Figure 15 indicates the onset of instability. The final figure clearly illustrates the transitional phase to turbulent flow. The time frame in which the pictures were taken was such that between Figures 14 and 16, 0.11 second elapsed, giving an indication of the speed with which the transition from laminar to turbulent flow progressed. This particular flow phenomena was only encountered once during the investigation and while the measured ε might indicate a Type II instability, the $\sqrt{R_{r_t}}$ calculated for this one particular test run was no different than the $\sqrt{R_{r_t}}$'s recorded for the expected instabilities on the same test body. Thus the exact reason why the nature of the flow field changed during this one particular test run remains unknown. Ironically, this run yielded the best photographic results obtained for the convex paraboloid in that it clearly showed the laminar flow regime being influenced by an instability and causing it to become turbulent.

SECTION IV
CONCLUSION

The data collected for the three different test bodies lead to the conclusion that the wall curvature of the convex and concave paraboloids did not alter the observed flow field significantly from that observed on the flat disk. The range of Reynolds numbers recorded for primary instability and transition to turbulence were found to be comparable in all three cases when the corrected values for the non-flat test bodies were used. The angle ε_c was found to be generally smaller on the paraboloids than the flat disk and no predictable variation of ε_c with local Reynolds number, as observed on the flat test body, was detected for either the concave or convex paraboloids for reasons discussed earlier.

The range of Reynolds numbers for the onset of primary instability and transition to turbulence calculated for the flat disk was also found to be smaller than earlier tests[13] reported. The discrepancy is probably due to the shallowness of the water tank or the different visualization technique employed.

Finally, the appearance of Type II instabilities during two test runs of the flat disk clearly showed these instabilities to exist up to a Reynolds number at which the primary instabilities appeared and to interfere destructively with these. The anomaly observed under the convex paraboloid was probably not a Type II instability and reinforces the belief that further investigation is necessary to establish fully the flow field present under rotating disks and paraboloids.

Table 1. Comparison of Data

Source	Onset of Primary Instability		Transition to Turbulence	ε	$\bar{\lambda}_\alpha$	α	Investigative Method
	R_c	$\sqrt{R_{r_o}}$	$\sqrt{R_{r_t}}$				
Gregory et al.	98-106	427-460	520-547	14°	17.5	.36	China-Clay
Faller & Kaylor	-	-	400	-	17.3	.36	
Chin & Litt	95-110	412-480	548-592	-	-	-	Electrochemical Probe
Tobak	-	-	-	11°	15	.4	Numerical
Clarkson et al.	122-143	532-621	562-680	11°	15	.4	Dye Injection
Malik et al.	-	294	513-526	-	-	-	Hot-Wire Probe
Kobayashi	-	297	566	-	-	-	Titanium Tetrachloride
Present Results							
Flat Disk	101-114	438-494	524-550	a	a	a	Aluminum Particle
Concave Paraboloid	84-99	365-432	514-546	a	a	a	Dye-Injection
Convex Paraboloid	87-118	377-515	453-608	a	a	a	Dye-Injection

a - See Tables 5, 6 and 7.

Table 2. Recorded Data for Flat Disk

Test Run	η	ζ	ε_m	λ_ϕ	r_o	r_t
1	15/59	182/.25	12.0	2.41	10.0	11.0
1	16/63	182/.25	10.5	2.81	10.0	10.8
1	15/59	182/.25	11.0	3.50	10.1	11.0
2	14/55	176/.25	13.0	2.70	10.0	11.0
2	14/55	176/.25	10.0	2.80	10.0	11.1
2	15/59	176/.25	11.0	2.80	9.9	11.0
3	7/19	70/.25	9.0	3.10	7.1	8.3
4	11/28	63/.25	8.5	3.30	7.0	8.2
5	3/ 8	49/.25	8.0	4.20	6.0	6.9
6	3/ 8	28/.25	7.5	6.25	4.3	5.2

Table 3. Recorded Data for Concave Paraboloid

Test Run	η	ζ	ε_m	λ_ϕ	r_o	r_t
1	12/35	78/.25	7	3.5	6	-
1	12/35	78/.25	6	3.5	6	-
1	12/35	78/.25	5	3.5	6	-
2	12/35	47/.25	8	4.7	4.7	5.7
2	12/35	47/.25	5	5.0	4.7	6.0
2	12/38	47/.25	7	4.7	4.2	5.8

Table 4. Recorded Data for Convex Paraboloid

Test Run	η	ζ	ε_m	λ_ϕ	r_o	r_t
1	13/38	99/.25	7	3.8	6.0	7.0
1	13/38	99/.25	6	4.6	6.1	7.5
1	13/38	99/.25	7	4.6	6.0	7.3
2	12/35	96/.25	6	4.4	6.1	7.4
3	11/35	109/.25	-6	-	-	7.3
4	12/35	73/.25	6	4.2	6.0	6.8
4	13/38	73/.25	7	4.2	5.9	6.8
5	12/36	40/.25	6	5.3	5.2	6.2
6	13/38	53/.25	7	5.0	6.0	6.9

Table 5. Calculated Data for Flat Disk

Test Run	R_c	$\sqrt{R_{r_o}}$	$\sqrt{R_{r_t}}$	ε_m	α	$\bar{\lambda}_\alpha$
1	112	486	534	12.0	.40	15.5
1	112	486	524	10.5	.47	13.4
1	113	490	534	11.0	.59	10.7
2	114	494	543	13.0	.45	14.0
2	112	493	550	10.0	.46	13.6
2	112	488	543	11.0	.46	13.6
3	106	462	540	9.0	.39	16.3
4	107	465	544	8.5	.40	15.7
5	106	462	532	8.0	.44	14.3
6	101	438	530	7.0	.49	12.7

Table 6. Calculated Data for Concave Paraboloid

Test Run	Measured Values						Corrected Values			
	R_c	$\sqrt{R_{r_o}}$	$\sqrt{R_{r_t}}$	ϵ_m	$\bar{\lambda}_\alpha$	α	R_c	$\sqrt{R_{r_o}}$	$\sqrt{R_{r_t}}$	ϵ_c
1	88	383	-	7	15.8	.40	97	424	-	9.1
1	90	390	-	6	16.1	.39	99	432	-	7.8
1	90	390	-	5	15.8	.40	99	432	-	6.2
2	89	387	469	8	14.7	.43	95	413	514	9.9
2	89	387	494	5	13.8	.46	95	413	546	6.2
2	80	346	478	7	14.5	.43	84	365	525	8.5

Table 7. Calculated Data for Convex Paraboloid

Test Run	Measured Values						Corrected Values			
	R_c	$\sqrt{R_{r_o}}$	$\sqrt{R_{r_t}}$	ϵ_m	$\bar{\lambda}_\alpha$	α	R_c	$\sqrt{R_{r_o}}$	$\sqrt{R_{r_t}}$	ϵ_c
1	78	341	397	7	12.8	.49	87	377	453	9.4
1	80	346	426	6	10.7	.59	88	384	493	8.2
1	78	340	414	7	10.6	.59	87	377	477	9.5
2	81	351	431	6	11.3	.55	90	390	500	8.2
3	-	-	394	-6	-	-	-	-	454	-8.5
4	91	396	449	6	13.6	.46	101	438	509	8.0

Table 7.--continued

Test Run	Measured Values						Corrected Values			
	R_c	$\sqrt{R_{r_o}}$	$\sqrt{R_{r_t}}$	ε_m	$\overline{\lambda}_\alpha$	α	R_c	$\sqrt{R_{r_o}}$	$\sqrt{R_{r_t}}$	α
4	90	390	449	7	13.6	.46	99	430	509	9.3
5	108	470	561	6	14.6	.43	117	508	624	7.7
6	107	465	535	7	13.4	.46	118	514	608	9.4

Table 8. Variation of ε_c with radius for a measured ε_m of 10 Degrees

r_o (In.)	ε_m (Deg.)	ε_c (Deg.)
1	10	10.00
2	10	10.27
3	10	10.71
4	10	11.29
5	10	12.00
6	10	12.80
7	10	13.68
8	10	14.26

Table 9. Radius r_o versus Arc Length s_o

r_o (In.)	s_o (In.)
0	0.0
1	1.0
2	2.03
3	3.08
4	4.20
5	5.38
6	6.64
7	7.98
8	9.43

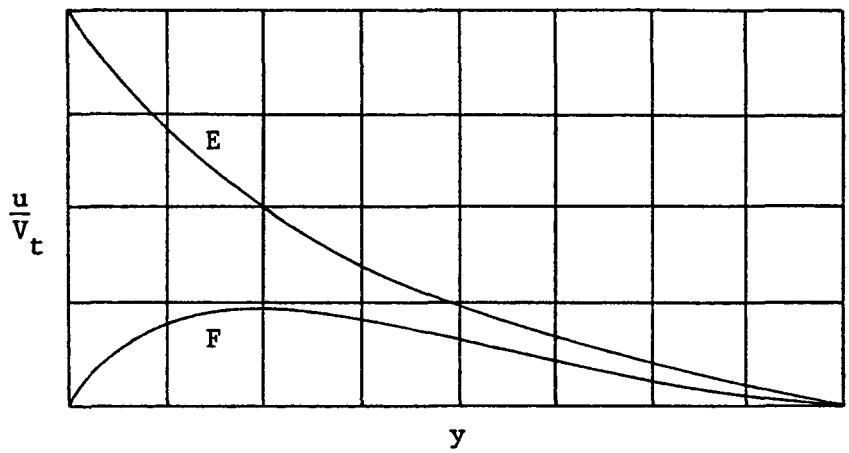

F - Boundary Layer profile in the radial direction

E - Boundary Layer profile in the tangential direction

Figure 1. Velocity Distribution near a Rotating Disk (Source: Ref. 1)

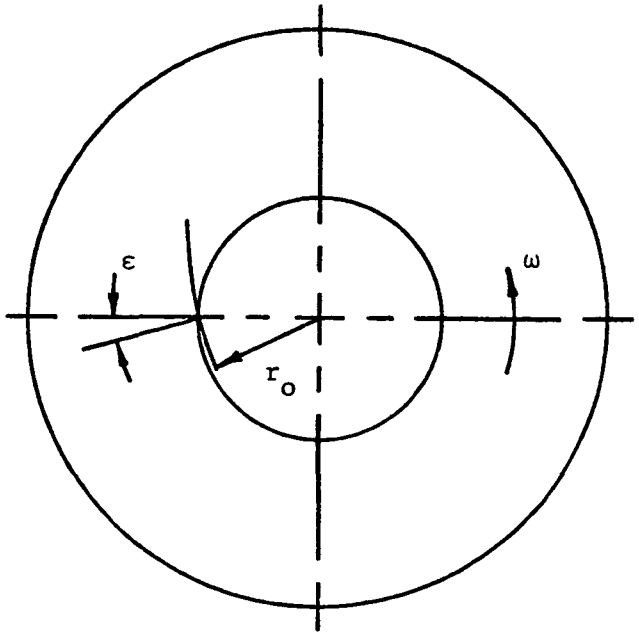

Figure 2. Schematic of Vortex Pattern

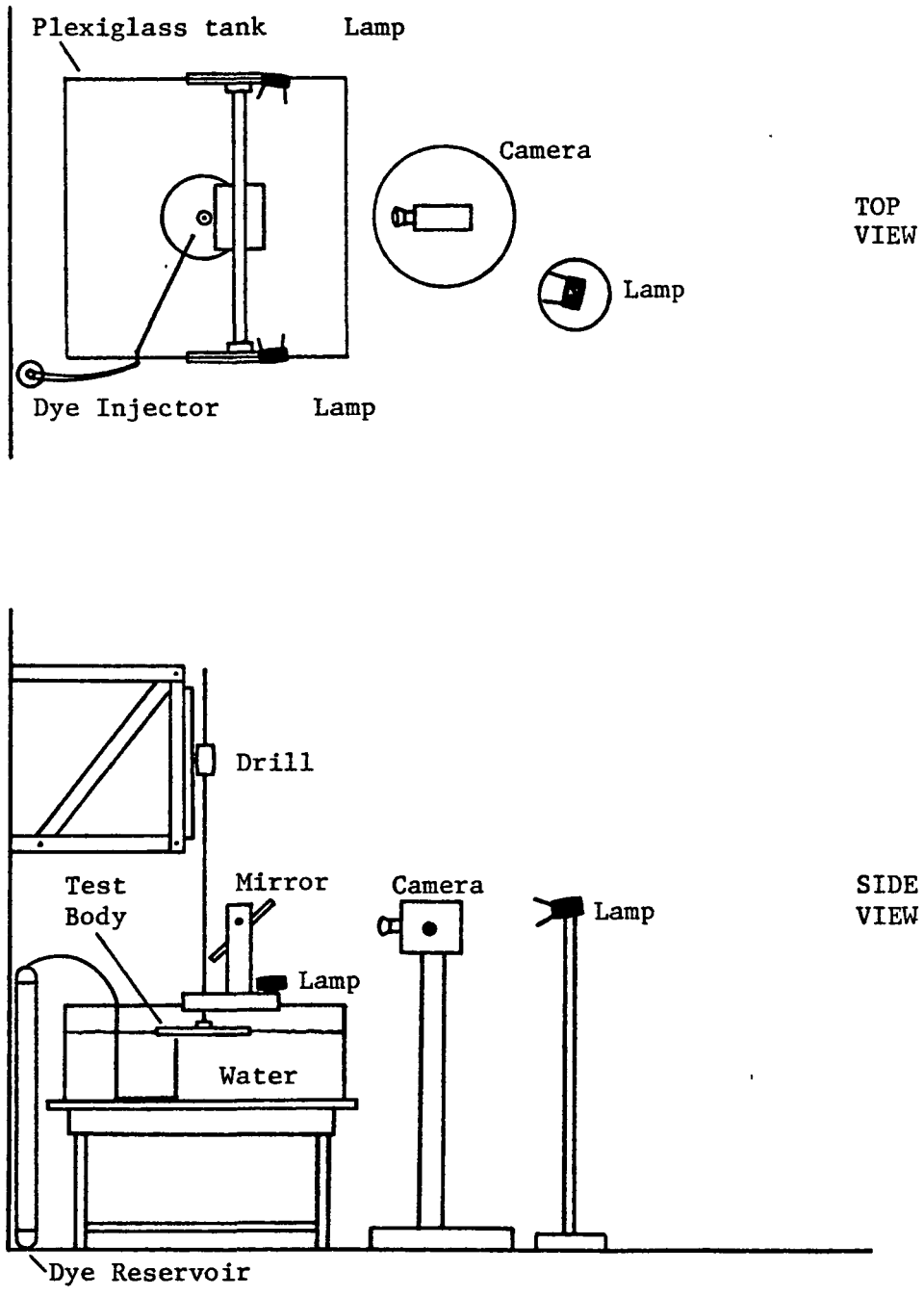

Figure 3. Experimental Apparatus

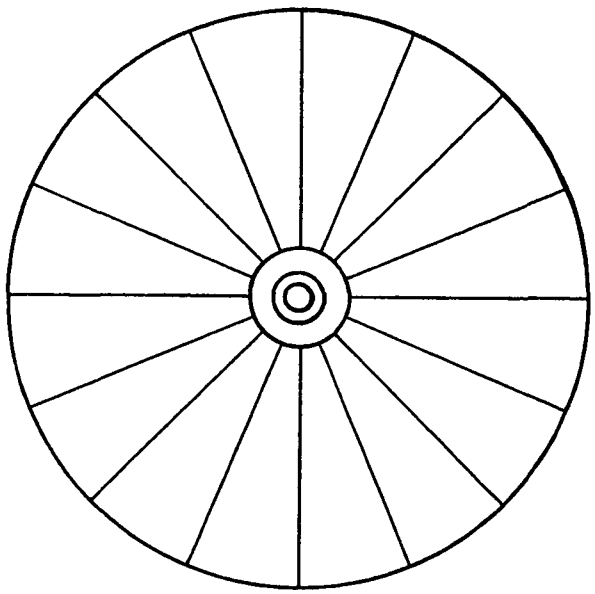

d = 24 in.
t = .5 in.

Figure 4. Flat Disk

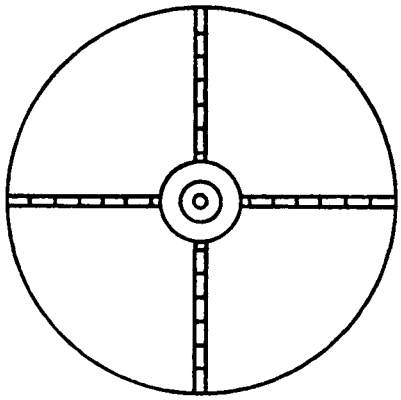

$$y = 4.444-(6.944\times10^{-2})r^2$$

$$t = 5.5 \text{ in.}$$

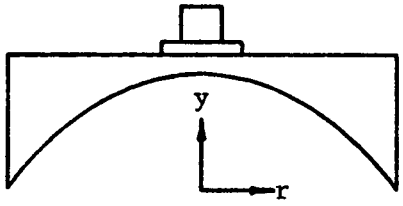

Figure 5. Concave Paraboloid

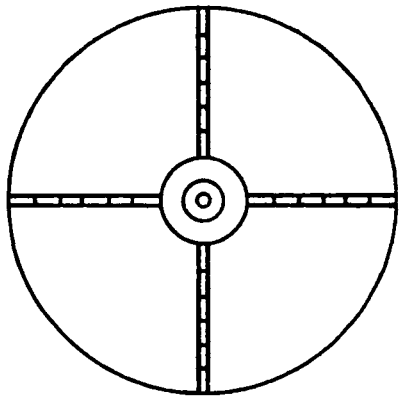

$y = 6.9444 \times 10^{-2} r^2$

$t = 5.75$ in.

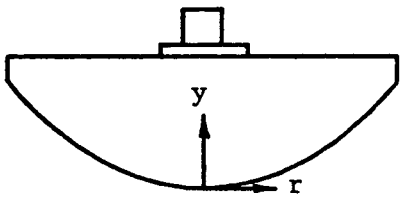

Figure 6. Convex Paraboloid

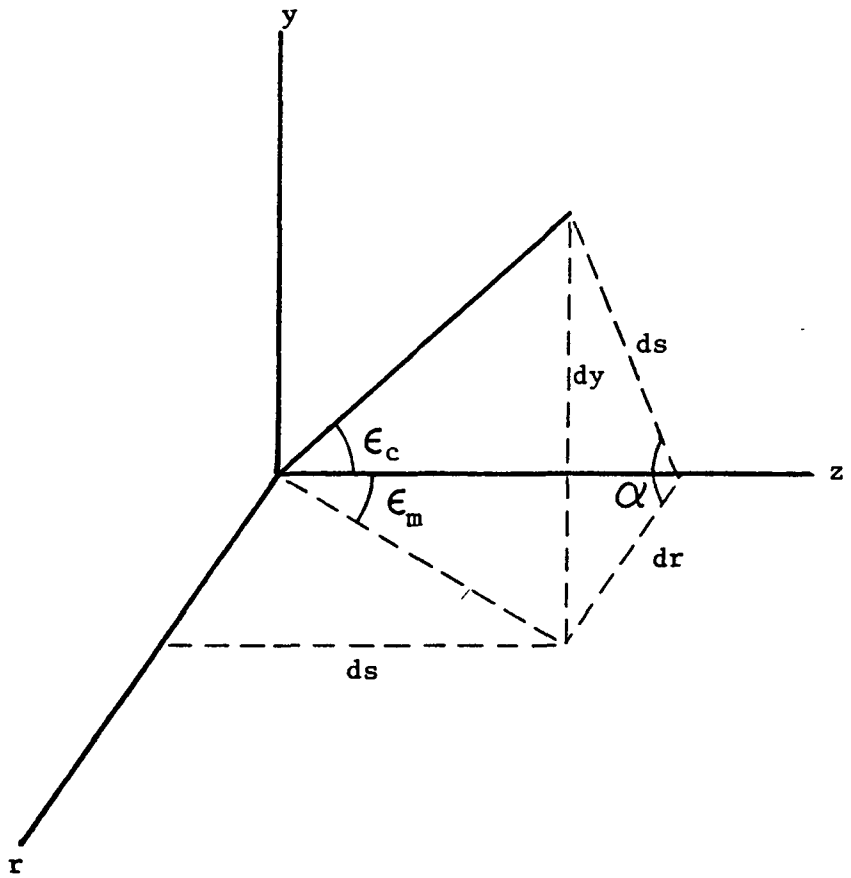

Figure 7. Angle ε Correction

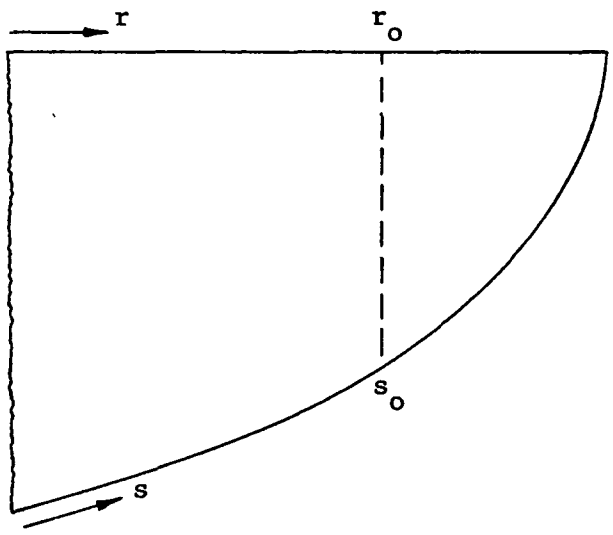

Figure 8. Variation of Arc Length s with Radial Distance r

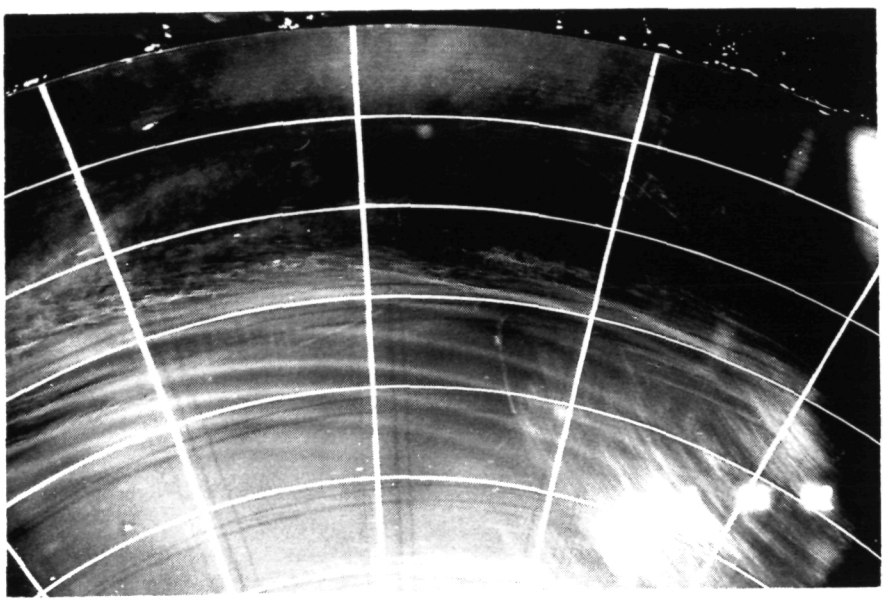

Figure 9. Vortex Pattern as observed under Rotating Flat Disk

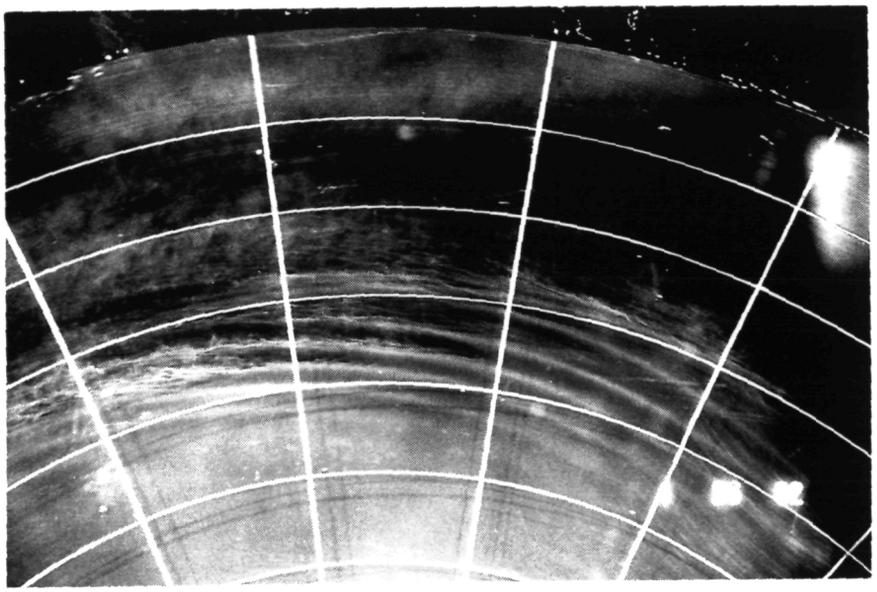

Figure 10. Variation of Transition to Turbulence Radii on the Flat Disk

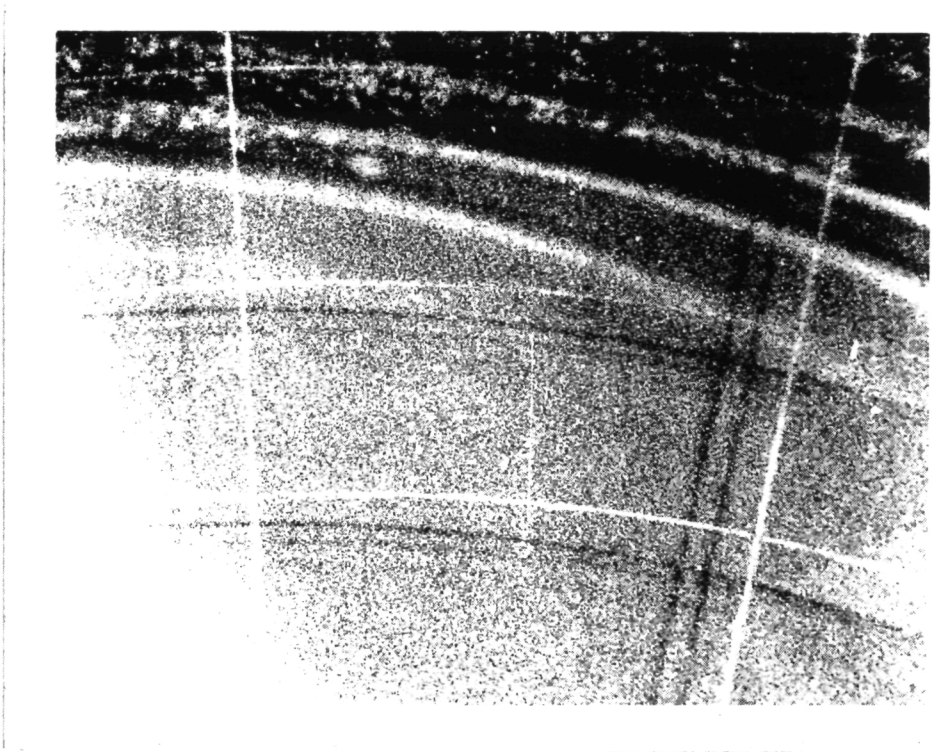

Figure 11. Variation of Circumferential Vortex Spacing with Radius

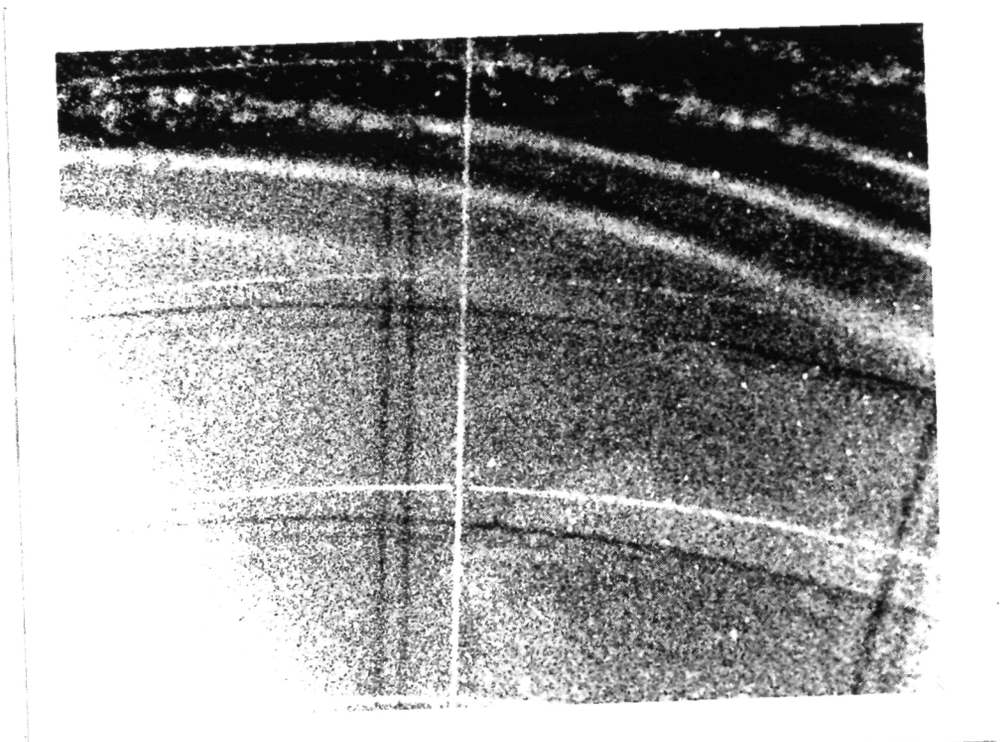

Figure 12. Vortex Visualization by Aluminum Powder-Water Mixture

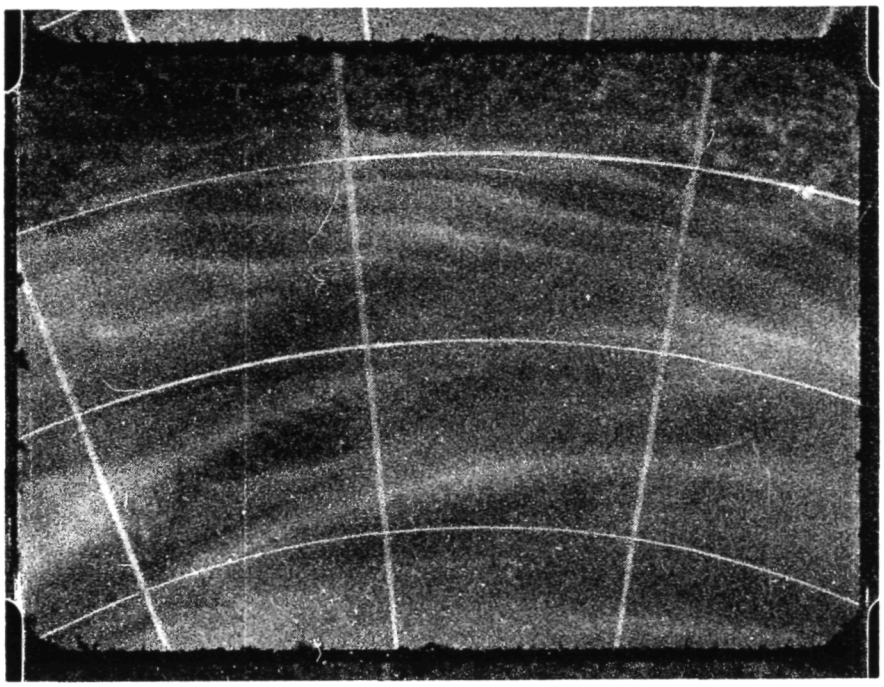

Figure 13. Simultaneous Occurrence of Type II and Inflexional Instabilities

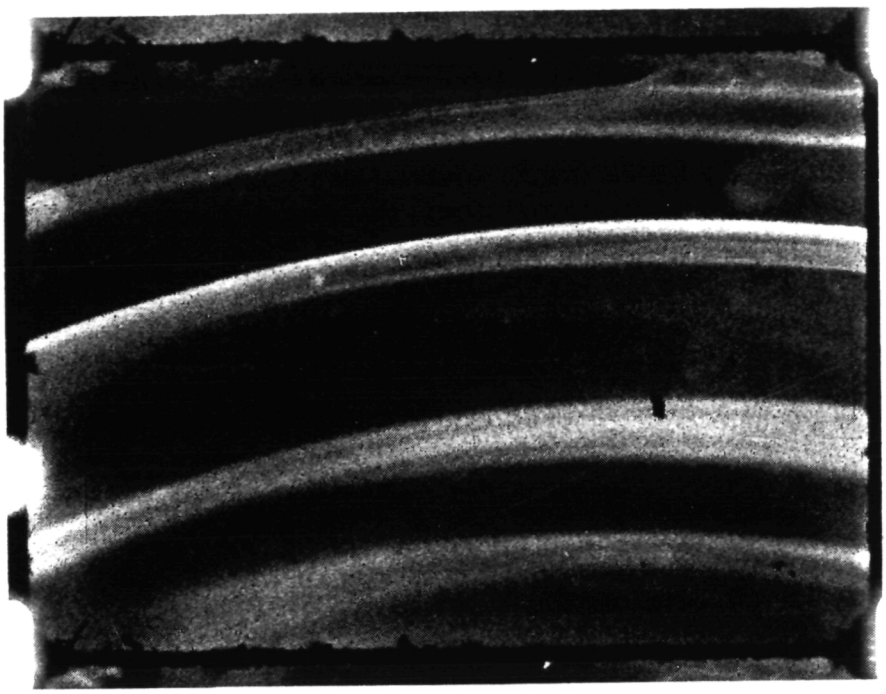

Figure 14. Laminar Flow under Convex Paraboloid

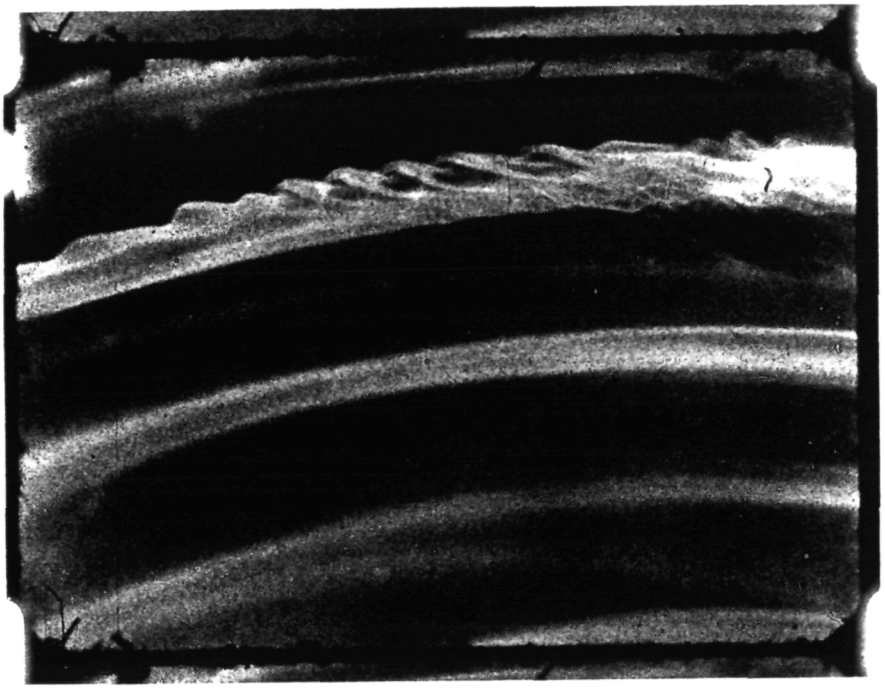

Figure 15. Transition of Flow Field to Turbulence under the Convex Paraboloid

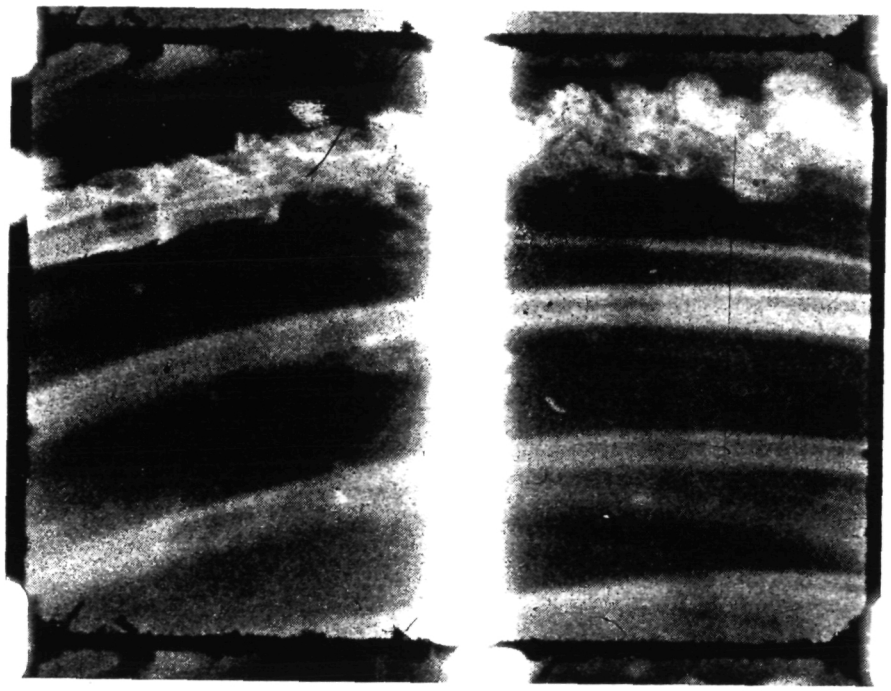

Figure 16. Fully Developed Turbulent Flow under the Convex Paraboloid

REFERENCES

1. Schlichting, H., "Boundary Layer Theory," McGraw-Hill Book Company, New York, 1966, pp. 93-94.

2. Schlichting, H., "Boundary Layer Theory," McGraw-Hill Book Company, New York, 1966, p. 95.

3. Smith, N. H.,"Exploratory Investigation of Laminar Boundary Layer Oscillations on a Rotating Disk," NACA TN 1227, 1947.

4. Gray, W. E., "The Effect of Wing Sweep on Laminar Flow," RAE Technical Memo. No. 255, ARC No. 14,929.

5. Owen, P. R. and Randall, D. G., "Boundary Layer Transition on a Swept Back Wing," RAE Technical Memo. Aero. 277, May 1952.

6. Gregory, N., Stuart, J. T. and Walker, W. E., "On the Stability of three-dimensional Boundary Layer with applications to the Flow due to a Rotating Disk," Philosophical Transactions of the Royal Society of London, Series A, Vol. 248, No. 943, July 1955, pp. 155-199.

7. Faller, A. J. and Kaylor, R. E., "Investigations of Stability and Transition in Rotating Boundary Layers," Dynamics of Fluids and Plasmas, edited by S. I. Pai, Academic Press, New York, 1966 pp. 309-329.

8. Chin, D. T. and Litt, M., "Mass Transfer to Point Electrodes on the Surface of a Rotating Disk," Journal of the Electrochemical Society, Vol. 119, Oct. 1972, pp. 1338-1343.

9. Kobayashi, R., Kohama, Y., and Takamadate, Ch., "Spiral Vortices in Boundary Layer Transition Region on a Rotating Disk," Acta Mechanica, Vol. 35, 1980 pp. 71-82.

10. Malik, M. R., Wilkinson, S. P., and Orszag, S. A., "Instability and Transition in Rotating Disk Flow," AIAA Journal, Vol. 19, No. 9, September 1981, pp. 1131-1138.

11. Brown, W. B., "Numerical Calculation of the Stability of Cross-flow Profiles in Laminar Boundary Layers on a Rotating Disc and on a swept-back Wing and an Exact Calculation of the Stability of the Blasius Velocity Profile," Northrop Aircraft Rept. NAI-59-5, Jan. 1959.

12. Tobak, M., "On Local Inflexional Instability in Boundary-Layer Flows," Zeitschrift fuer Angewandte Mathematik und Physik, Vol. 24, 1973, pp. 330-354.

13. Clarkson, M. H., Chin, S. C., and Shacter, P., "Visualization of Flow Instabilities an a Rotating Disk," AIAA Journal, Vol. 18, No. 12, Dec. 1980, pp. 1541-1543.